BBA - Biomembranes 1860 (2018) 300–309

Contents lists available at ScienceDirect

BBA - Biomembranes

journal homepage: www.elsevier.com/locate/bbamem

Effect of phosphatidylcholine bilayer thickness and molecular order on the binding of the antimicrobial peptide maculatin 1.1

Tzong-Hsien Lee[a], Marc-Antoine Sani[b], Sarah Overall[b], Frances Separovic[b], Marie-Isabel Aguilar[a,*]

[a] Biomedicine Discovery Institute and Department of Biochemistry and Molecular Biology, Monash University, Clayton, VIC 3800, Australia
[b] School of Chemistry, Bio21 Institute, University of Melbourne, Melbourne, VIC 3010, Australia

ARTICLE INFO

Keywords:
Frog antimicrobial peptides
Maculatin
Dual polarisation interferometry
Solid-state NMR
Membrane thickness

ABSTRACT

Antimicrobial peptides (AMPs) interact directly with bacterial membrane lipids. Thus, changes in the lipid composition of bacterial membranes can have profound effects on the activity of AMPs. In order to understand the effect of bilayer thickness and molecular order on the activity of AMPs, the interaction of maculatin 1.1 (Mac1.1) with phosphatidylcholine (PC) model membranes composed of different monounsaturated acyl chain lengths between 14 and 22 carbons was characterised by dual polarisation interferometry (DPI) and 31P and 1H solid-state NMR techniques. The thickness and bilayer order of each PC bilayer showed a linear dependence on the acyl chain length. The binding of Mac1.1 exhibited a biphasic dependency between the amount of bound Mac1.1 and bilayer thickness, whereby the mass of bound peptide increased from C14 to C16 and then decreased from C16 to C22. Significant perturbation of 31P chemical shift anisotropy (CSA) values was only observed for DOPC (C18) and DEPC (C22), respectively. In the case of DEPC, the greater range in CSA indicated different headgroup conformations or environments in the presence of Mac1.1. Overall, the results indicated that there is a significant change in the bilayer order upon binding of Mac1.1 and this change occurred in a co-operative manner at higher concentrations of Mac1.1 with increasing bilayer thickness and order. Overall, an optimum bilayer thickness and lipid order may be required for effective membrane perturbation by Mac1.1 and increasing the bilayer thickness and order may counteract the activity of Mac1.1 and play a role in antimicrobial resistance to AMPs.

1. Introduction

The increasing rate of bacterial resistance to conventional antibiotics in recent years is one of the most significant threats to health globally and requires urgent solutions [1]. Many factors contributing to our current understanding of the mechanisms of antimicrobial resistance are related to the emergence of resistance, transmission, bacterial fitness and potential for reversibility upon withdrawing the drug [2]. Solutions to control and reduce the emergence and spread of drug-resistant bacterial infections remain as major challenges [3]. Various alternative antibacterial technologies, including antibiotic biomaterials [4], antimicrobial nanoparticles [5,6], antimicrobial peptides [7,8], anti-virulence materials [9,10], bacteriophages [11,12], vaccines and therapeutic antibiotics [12–14], are being developed in an attempt to complement conventional antibiotics for clinical uses. Amongst these technologies, antimicrobial peptides (AMPs) show increasing promise with a broad antibacterial spectrum and potential as a combination therapy [7,8,12].

Various molecular mechanisms have been described for the antibacterial activities of AMPs which mainly target the bacterial membrane causing changes in permeability or destruction through the formation of pores, membrane thinning, or detergent-like micellization [15]. In addition, the interaction of AMPs with the bacterial membrane can also induce membrane perturbation by forming specific domains, non-lamellar phases and lateral phase segregation. The selective activities of AMPs targeted to bacteria are strongly influenced by the lipid composition of bacterial membranes where the negatively charged phospholipids play a prominent role in promoting peptide binding and insertion into the membrane [16]. In contrast, peptides bind primarily at the interfacial region of bilayers consisting solely of zwitterionic lipids.

Since the isolation of AMP-resistant bacteria, investigations have begun to gain insights into the mechanisms of AMP-resistance [17–19]. Several putative mechanisms counteracting the antibacterial activities

* Corresponding author. at: Department of Biochemistry and Molecular Biology, Monash University, Wellington Rd, Clayton, VIC 3800, Australia.
E-mail address: Mibel.Aguilar@monash.edu (M.-I. Aguilar).

https://doi.org/10.1016/j.bbamem.2017.10.007
Received 10 August 2017; Received in revised form 18 September 2017; Accepted 8 October 2017
Available online 11 October 2017

of AMPs have been identified that mainly relate to phenotypic changes in membranes [17–19]. These changes include thickening of the cell wall, modification of the phospholipid composition, reducing the net surface charge, adjusting the membrane fluidity or rigidity, and changes in the membrane thickness, which all affect the physicochemical properties of the membrane [18–23]. For example, modification of fatty acids by increased level of longer and more unsaturated acyl chains in bacterial membrane lipids has been reported for *Staphylococcus aureus* in response to platelet-derived AMPs and class IIa bacteriocin [24,25], and for *Enterococcus faecalis* to daptomycin and other AMPs [22,26]. Although changes in the fatty acyl chain length and unsaturation alter membrane fluidity, it is not clear how these compositional changes affect bacterial membrane properties and resistance to AMPs. Therefore, studying the effect of acyl chain composition on the activity of AMPs is important in understanding the role of membrane structure in regulating the activity/resistance of AMPs.

Maculatin 1.1 (GLFGVLAKVAAHVVPAIAEHF-NH_2) is a cationic AMP isolated from the skin secretions of the frog species *Litoria genimaculata* [27] and has antibacterial [27–32], antitumour [33] and antiviral [34] activity. Several studies have shown that maculatin 1.1 (Mac1.1) exerts a greater effect on model membranes composed of anionic dimyristoylphosphatidylglycerol (DMPG) bilayers [31,35–38] and also destabilises the gel-phase zwitterionic dimyristoylphosphocholine (DMPC) above a critical threshold for insertion and incremental expansion leading to membrane disruption [39–42]. The proline residue in Mac1.1 has also been shown to play an important role in facilitating membrane insertion as replacement of the Pro-15 residue results in a structural rearrangement into a tighter, more canonical α-helix with altered hydrophobicity and antimicrobial activity [43]. It has also been well established that the negative surface charge of a membrane plays a critical role in enhancing the binding and insertion of Mac1.1 and other AMPs [41,42]. But what is less well characterised is the role of acyl chain composition on the AMP activity as the acyl chain of bacterial membrane lipid can vary greatly in response to environmental pressure. Mismatch between the bilayer thickness and the peptide length can reduce the helical content of Mac1.1 in the presence of model membranes composed of PC with different acyl chain lengths [44]. This mismatch can also affect the possible oligomeric state of Mac1.1 inserted into the membrane with a higher number of peptide monomers found in thicker membranes [45]. Changes in the acyl chain length and degree of saturation, therefore, have profound effects on the binding mechanisms and orientation of AMPs upon binding to a membrane [44,46–48]. To further explore the effect of acyl chain composition on the interaction of Mac1.1 with a phospholipid membrane, the interaction of Mac1.1 with phosphatidylcholine (PC) bilayers composed of different monounsaturated acyl chain lengths between 14 and 22 carbons was characterised by dual polarisation interference (DPI) and solid-state NMR techniques. The concentration dependence of a membrane destabilization threshold for Mac1.1 on the bilayer thickness demonstrated that the increases in acyl chain length, bilayer thickness and lipid order impede insertion of Mac1.1 into the membrane.

2. Material and methods

2.1. Materials

Maculatin 1.1 was obtained from the Bio21 peptide synthesis facility (Melbourne, Australia) with > 95% purity. The peptide was washed in 5 mM HCl solution and lyophilized overnight to remove residual trifluoroacetic acid as described [46]. The peptide stock was then re-suspended in Milli-Q water and pH adjusted to 7.2 using concentrated ammonium hydroxide solution and lyophilized overnight.

1,2-Dierucoyl-*sn-glycero*-3-phosphocholine (DEPC; di-22:1 (Δ13-*cis*) PC), 1,2-dioleoyl-*sn-glycero*-3-phosphocholine (DOPC; di-18:1 (Δ9-*cis*) PC), 1,2-dipalmitoleoyl-*sn-glycero*-3-phosphocholine (DPoPC; di-16:1 (Δ9-*cis*) PC), and 1,2-dimyristoleoyl-*sn-glycero*-3-phosphocholine (DMoPC; di-14:1 (Δ9-*cis*) PC) were purchased from Avanti Polar Lipids (Alabaster, USA) and used without further purification.

2.2. Dual polarisation interferometry

Dual polarisation interferometry is an analytical method for analysing thin films using an alternate dual orthogonal polarisation [49]. The Analight BIO200 (Farfield Group Ltd., Manchester, UK) was used to measure the real-time changes of thickness, refractive index (RI), mass per unit area and birefringence for both bilayer formation and peptide binding. The real-time data were acquired with AnaLight200 version 2.1.0 software and processed and analyzed using AnaLight® Explorer software. Data were acquired at 10 Hz and averaged to give an output of one data point per second. The planar-supported unilamellar lipid bilayer was prepared on an unmodified silicon oxynitride FB80 AnaChips (Farfield-Group, UK). The chip surface was cleaned in situ by rinsing two times each with 10% Hellmanex II, 2% sodium dodecyl sulfate (SDS) and absolute ethanol. Prior to measurement, the waveguide chips were calibrated with an 80:20 w/w ethanol/water mixture at 20 °C. 10 mM HEPES pH 7.0, 150 mM NaCl was used as the bulk running buffer to all binding experiment. The flow rate of running buffer was controlled by a Harvard Apparatus PHD2000 programmable syringe pump.

2.3. In situ formation of supported lipid bilayer (SLB)

Liposomes were prepared by drying each 2 mM di-(Cn:1)-PC in chloroform under vacuum and rehydration of the PC thin film in running buffer (10 mM HEPES, 150 mM NaCl, pH 7.0) as previously described [41,50–52]. The liposome (0.15 mg/mL) solutions were injected in the presence of 1 mM $CaCl_2$ onto the chip at 20 μL/min at 28 °C for 10 min. The SLB was further stabilised and equilibrated in running buffer for 20 min before adjusting the temperature to 20 °C.

2.4. Peptide binding to bilayers

Peptide solutions were prepared at concentrations of 1.25, 2.5, 5, 10, 20 and 40 μM in 10 mM HEPES, pH 7.4, 150 mM NaCl. 160 μL of each peptide solution were injected consecutively in order of 2-fold incremental concentration onto the deposited bilayer at a flow rate of 40 μL/min at 20 °C. At the end of each injection, the layer was equilibrated for 30 min prior to injecting the next concentration onto the same bilayer surface. Each concentration measurement was performed on the same lipid bilayer for each analogue. At the end of all peptide binding, the waveguide surface was regenerated with 2% SDS, 10% Hellmanex II and ethanol at 28 °C.

2.5. Calculation of mass and birefringence (Δn_f)

The mass of an adsorbed molecular layer was calculated using the de Feijter formula [53,54]. The mass of lipid bilayer (m_{lipid}) formed on the solid support, and the mass of peptide ($m_{peptide}$) bound to the lipid bilayer, are calculated as follows:

$$m_{lipid} = d_f (n_{iso} - n_{buffer})/(dn/dc)_{lipid}, \quad (1)$$

$$m_{peptide} = d_f (n_{iso} - n_{buffer})/(dn/dc)_{peptide}, \quad (2)$$

where d_f is the thickness of the adlayer, and n_{iso} denotes the average or corresponding isotropic RI of the adlayer:

$$n_{iso} = \sqrt{(n_{TM}^2 + 2n_{TE}^2)/3} \quad (3)$$

n_{buffer} is the RI of the HEPES buffer used for these experiments, which was obtained experimentally as $n_{buffer} = 1.3349$ (20 °C); c is concentration, and dn/dc is the specific RI increment of the adlayer. The de Feijter formula assumes that dn/dc remains constant throughout the

Table 1
The structural parameters of supported di-monounsaturated phosphatidylcholine (di-(Cn:1)-PC) bilayer with acyl chain lengths from 14 to 22 carbons at 20 °C.

	Lipid	Acyl chain length	MW	Thickness (nm)	Δn_f	Mass (ng/mm^2)	Area/lipid (Å^2)
1	DMoPC	14:1/14:1	673.9	3.86 ± 0.02	0.0149 ± 0.0001	3.87 ± 0.02	57.82 ± 0.30
2	DPoPC	16:1/16:1	730.0	4.20 ± 0.01	0.0145 ± 0.0001	4.21 ± 0.01	57.58 ± 0.14
3	DOPC	18:1/18:1	785.6	4.37 ± 0.02	0.0165 ± 0.0001	4.37 ± 0.02	59.69 ± 0.27
4	DEPC	22:1/22:1	898.3	5.41 ± 0.06	0.0186 ± 0.0002	5.41 ± 0.06	55.20 ± 0.61

experiment. For the present analysis, the *dn/dc* values of 0.135 mL/g and 0.182 mL/g were used for lipids and peptides, respectively [41,50,51].

The degree of molecular order, S, of the uniaxial lipid bilayer is defined by the ratio of the principal polarisabilities of the bilayer to the molecular polarisabilities [55,56]. This order parameter (S) is proportional to the birefringence (Δn_f) values. The birefringence of the adsorbed planar bilayer is obtained using DPI by calculating the difference between two effective RIs, namely RI of transverse magnetic (TM) waveguide mode (n_{TM}) and RI of transverse electric (TE) waveguide mode (n_{TE}), as described previously [52]. The effective birefringence (n_{TM} - n_{TE}) was determined by calculating the two RIs, n_{TM} and n_{TE}, for each waveguide mode by fixing the RI at 1.47 for the supported lipid bilayer formation at 20 °C [52].

2.6. NMR sample preparation

Maculatin 1.1 was first solubilized in trifluoroethanol (TFE) and transferred to the phospholipid system dissolved in chloroform (final $CHCl_3$/TFE 1:1 volume) to reach a lipid to peptide molar ratio of 25:1. The peptide-free samples were solubilized in chloroform/TFE. The organic solvent was removed under argon flow and the samples were further dried under vacuum overnight. The dry samples were re-suspended in buffer solution (20 mM imidazole, 50 mM KCl, 1.8 mM EDTA, pH 7.4) to obtain a hydration level of 80% by weight water. Four freeze-thaw cycles were performed before packing the sample into a 4 mm zirconia rotor with a Teflon spinning cap for NMR experiments.

2.7. ^{31}P solid-state NMR

The ^{31}P experiments were conducted at 25 °C on a Bruker 400 MHz NMR equipped with HXY 4 mm MAS probe.^{31}P static and magic angle spinning (MAS) experiments were performed at 161 MHz, using a ca. 50 kHz single pulse excitation with ca. 60 kHz SPINAL64 ^1H decoupling [57], a 3 s recycle delay, a spectral width of 125 kHz, 8 k complex points acquisition zero-filled to 16 k points and line broadening ranging from 25 Hz to 100 Hz. Spectra were externally referenced to 0 ppm using H_3PO_4 prior to each MAS experiment. Phosphorus MAS experiments were acquired with proton decoupling using a single-pulse experiment and static spectra were acquired using a Hahn echo pulse sequence with Exorcycle phase cycling on the π pulse [58]. T_1 and T_2 relaxation experiments were performed at 8 kHz spinning speed using an inversion-recovery pulse sequence and a Hahn echo pulse sequence with Exorcycle phase cycling on the π pulse, respectively [59]. T_1 and T_2 values were obtained from single exponential fitting of the ^{31}P single resonance intensity using Gnuplot 4.6 (http://www.gnuplot.info) in-built least-squares fitting functionality.

Chemical shift anisotropy (CSA) and asymmetry (η) parameters encoded in sidebands of slow-spinning ^{31}P MAS spectra were extracted by Boltzmann-type maximum entropy (MEMAS) sideband analysis [60] using software obtained from https://github.com/jdgehman/BS-MAS. Fluid-phase bilayer systems were analyzed at 900, 1400 and 1600 Hz spinning speeds, solving for CSA values between −6 and 8 kHz in 25 Hz increments, and η values between 0 and 0.5 in 0.025 increments. Crystallite orientations used for matrix element calculations involved 2000 combinations of α and β angles from SIMPSON [61] crystal files and 128 γ angles uniformly dispersed over 2π.

2.8. ^1H solid-state NMR

The ^1H experiments were conducted at 25 °C on a Bruker 400 MHz NMR equipped with HXY 4 mm MAS probe. ^1H MAS experiments were performed at 400 MHz using a ca. 65 kHz single pulse excitation, a 3 s recycle delay, a spectral width of 125 kHz, 32 k complex points acquisition zero-filled to 64 k points without line broadening.

3. Results

3.1. Structural characterization of PC bilayers with different acyl chain length

Establishing model membranes with consistent and quantitatively defined structural properties prior to peptide binding is critical for relating membrane structural properties to peptide binding and to examine the impact of peptides on the membrane structure. Planar supported di-monounsaturated phosphatidylcholine (di(Cn:1)-PC) bilayers with different acyl chain lengths were prepared by in situ vesicle-to-bilayer transformation in the presence of 2 mM $CaCl_2$. The process of vesicle deposition-to-bilayer formation was monitored by real time changes in the TM and TE phases [52,62].

The structural parameters of di(Cn:1)-PC bilayers determined at 20 °C are listed in Table 1. Values of the surface area per lipid molecule were calculated based on the mass per unit chip surface area for a defect-free unilamellar PC bilayer formed on the chip. The calculated thickness of each bilayer was similar to those values obtained by X-ray scattering and neutron scattering measurements of multilamellar lipid bilayers or vesicles at 30 °C [63–66]. It should be noted that the thickness determined by DPI in this study corresponds to the fully hydrated phospholipid chain plus the head group and can be directly compared to the values for DEPC reported by Kucerka et al. [63] who used X-ray scattering. By comparison, values reported by the same group using neutron scattering and X-ray scattering [62] correspond to the phosphate distance across the bilayer and are, therefore, less than those in Table 1. The calculated area per lipid for each di(Cn:1)-PC bilayer was lower than those reported from X-ray scattering and neutron scattering measurement and may result from the tightly packed lipid molecules on the solid substrate used in DPI.

The dependence of bilayer thickness on the acyl chain length is shown in Fig. 1 which shows a linear increase in bilayer thickness with acyl chain length [67] for the di(Cn:1)-PC bilayers. Using this linear relationship yields a value of 0.19 nm per carbon for the hydrocarbon region, which is the same value obtained by fitting a series of bilayer thickness parameters reported from X-ray and neutron scattering data [68]. Meanwhile, the obtained intercept of 1.11 nm is consistent with double the value reported for the hydrophilic/hydrophobic boundary positioned at 0.55 nm from the Gaussian distribution function of the phosphate group [69,70].

In addition to the overall bilayer thickness, the molecular order and packing of the lipid molecules was also measured as birefringence by DPI and the values for each bilayer are listed in Table 1. As evident in Fig. 1, there is a linear relationship of bilayer birefringence as function of acyl chain length for these di(Cn:1)-PC bilayers. This result indicates

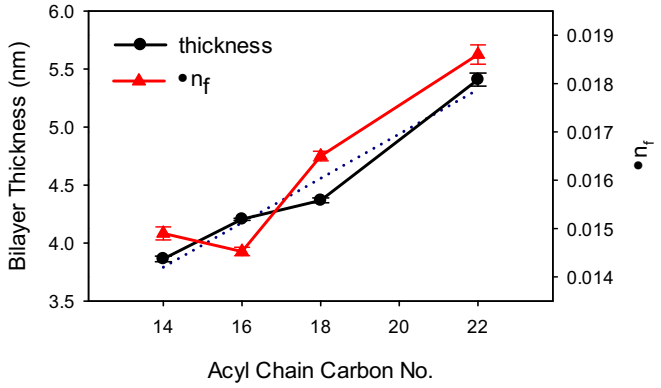

Fig. 1. The correlation of bilayer thickness and birefringence values as a function of acyl chain length for planar silicon oxynitride-supported DMoPC (14), DPoPC (16), DOPC (18), and DEPC (22) bilayers determined by DPI at 20 °C. The linear regression of this plot is shown as the dotted blue line with a slope of 0.19 nm/carbon, intercept of 1.11 nm and $R^2 = 0.963$.

that bilayers composed of longer acyl chain length lipids have higher chain packing, leading to higher orthogonal alignment of lipid molecules relative to the surface plane. Interestingly, a thickness of 4.37 ± 0.02 nm for DOPC is consistent with the thickness value previously reported in the presence of Ca^{2+} while the birefringence is closer to that obtained without Ca^{2+} [62]. In addition, the thickness of fully saturated DMPC (4.52 nm) [52,62,71] previously determined by DPI is also close to the thickness value of DOPC obtained in this study. However, the birefringence value was much higher for DMPC ($\Delta n_f = 0.022$, cf 0.0165 for DMoPC) indicating the decreased packing order in the presence of unsaturation, which can be quantitatively determined by the DPI.

3.2. Binding characteristics of Mac1.1 to PC bilayers of different thickness

The real-time changes in the lipid-bound m_p of Mac1.1 to PC bilayer with different thickness and packing order are shown in Fig. 2 for consecutive injections of 1.25, 2, 5, 10, 20 and 40 μM Mac1.1 onto the same bilayer. The injection of Mac1.1 at low concentrations (1.25 and 2.5 μM) resulted in small increases in m_p with slow initial binding while

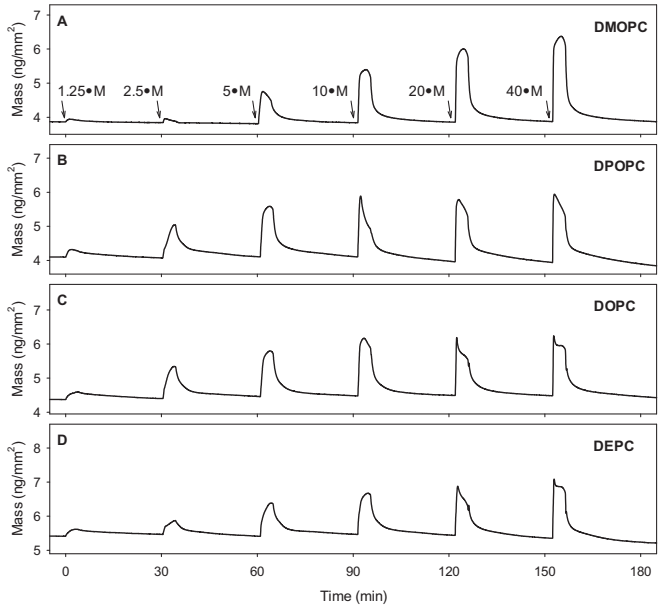

Fig. 2. The real-time changes of mass per unit area for Mac1.1 binding to: (A) DMoPC, (B) DPoPC, (C) DOPC, and (D) DEPC at concentration ranges from 1.25 to 40 μM labelled with arrows for the injection start of each concentration.

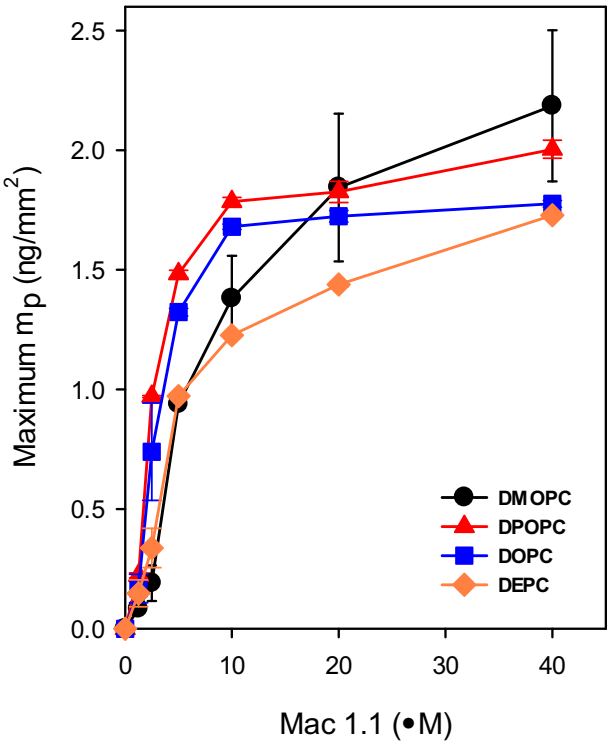

Fig. 3. The maximum mass per unit area of Mac1.1 binding to monounsaturated PC bilayers with acyl chain lengths between 14 and 22 carbons as a function of Mac1.1 concentration.

large increase in m_p with fast initial association to each PC bilayer was obtained at higher concentration (5 μM and above). At the end of peptide injection, Mac1.1 at low concentration dissociated to m_p values close to those prior to peptide injection. Small losses in m_p were observed at the end of dissociation at higher concentrations which resulted in net loss of mass compared to the pre-bound membrane mass for the longer acyl chain PC starting for 10 μM Mac1.1 on DPoPC (Fig. 2B), 10–20 μM Mac1.1 on DOPC (Fig. 2C) and 20 μM Mac1.1 to DEPC (Fig. 2D). The concentration threshold for the mass loss during the association thus increased with increasing bilayer thickness and molecular order.

The maximum m_p (m_pMax) binding to each PC bilayer as a function of Mac1.1 concentration is shown in Fig. 3 and shows a non-linear biphasic relationship. An initial linear dependence of m_pMax on Mac1.1 concentration was obtained from 1.25 to 5 μM for binding to all PC bilayers. Between 10 and 40 μM Mac1.1, the values of m_pMax plateaued for binding to DPoPC and DOPC bilayers, while the values continued to increase without a plateau for DMoPC and DEPC. In addition, at lower peptide concentrations up to 10 μM, Mac1.1 bound more to DPoPC and DOPC than to DMoPC and DEPC. The overall m_pMax obtained at 40 μM was inversely related to the bilayer thickness, with the lowest m_p to DEPC and the highest m_p to DMoPC. These results indicate that at the lower concentrations, a greater amount of Mac1.1 bound and reached saturation level for PC bilayers with 16–18 carbons, which may reflect a better match between the peptide length and the hydrophobic thickness. By comparison, an increase in the acyl chain length to 22 carbons significantly reduced the amount of Mac1.1 binding to the PC bilayers, and more peptide bound to the short chain DMoPC at higher concentrations.

3.3. Influence of lipid packing order on Mac1.1 induced-bilayer disordering

Characterizing the coherent dynamic changes with peptide structure and orientation is central to describing the molecular mechanism of AMP action associated with membrane surface binding, insertion and

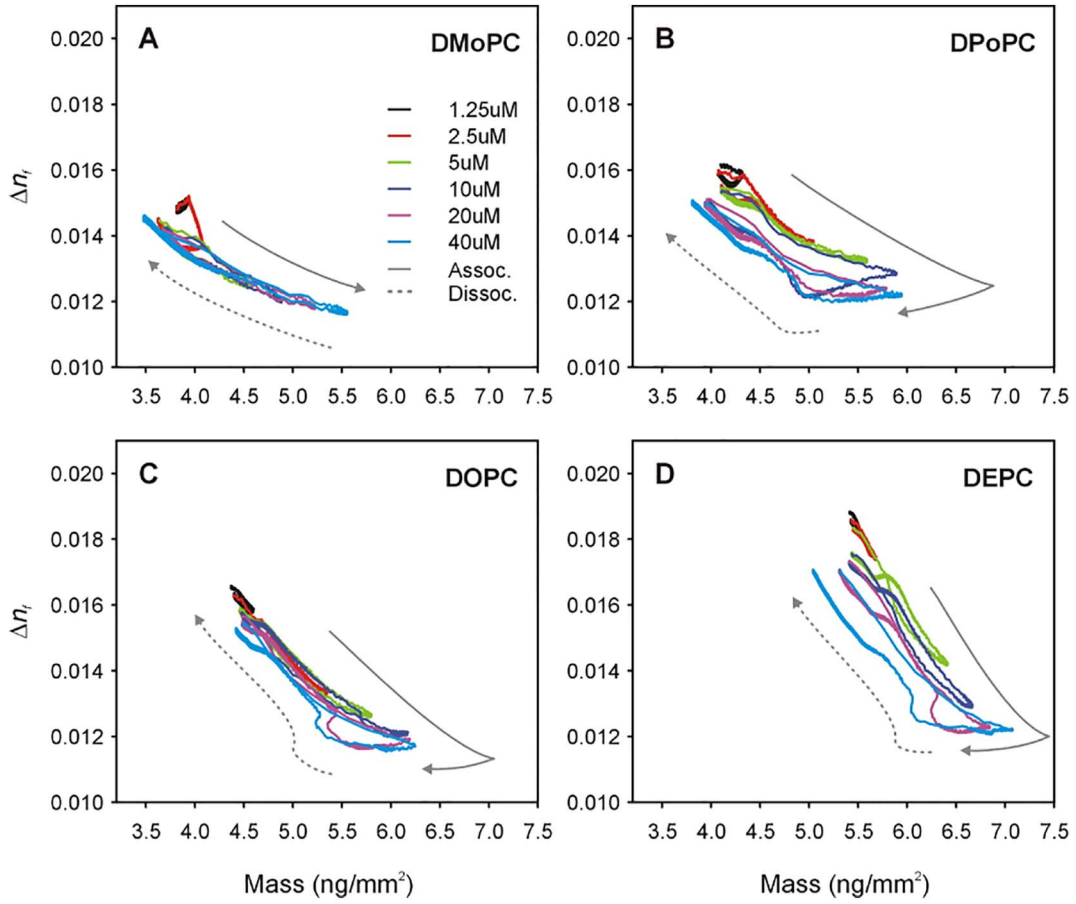

Fig. 4. The correlation of bilayer bound-Mac1.1 mass per unit area with changes in the molecular order (Δn_f) of: (A) DMoPC, (B) DPoPC, (C) DOPC, and (D) DEPC for Mac1.1 concentration range of 1.2 to 40 μM. The solid grey arrow indicates the association phase, while the dashed grey arrows denote the dissociation phase. Two transitions are evident in the association phase by the change in direction of the plot which occurs that define three stages of cooperative changes in bilayer disorder.

disruption. The changes in bilayer order throughout Mac1.1 association and dissociation were quantitatively examined by the simultaneous measurement of bilayer birefringence (Δn_f) and membrane-bound peptide mass per unit area (m_p) in real time. A decrease in Δn_f corresponds to membrane structural changes from ordered to disordered states [52]. Changes in the bilayer order as a function of m_p for Mac1.1 binding to the PC bilayers of different acyl chain length are shown in Fig. 4, and allow the impact of peptide binding on the membrane structure to be determined. The binding of 1.25 μM Mac1.1 to the lower ordered DMoPC resulted in small increases in Δn_f values at a low m_p, indicating that DMoPC became more ordered upon peptide binding (Fig. 4A). This small increase in order for DMoPC then returned to its initial value after Mac1.1 dissociated from the membrane. In contrast, a small initial increase followed by an abrupt decrease in Δn_f was observed during association of 2.5 ΔM Mac1.1 to DMoPC and was accompanied by a small mass loss. Further injection of 5–40 μM Mac1.1 showed decreases in Δn_f with increases in m_p which were fully reversible (as for 2.5 μM Mac1.1).

Initially, there was no change in the Δn_f for the binding of 1.25 μM Mac1.1 to DPoPC, but was followed by a small decrease as the m_p reached its maximum (Fig. 4B). The Δn_f returned to the initial state when Mac1.1 dissociated from the DPoPC. Further injection of 2.5 and 5 μM Mac1.1 to DPoPC resulted in a significant decrease in Δn_f with increasing m_p and these Δn_f changes were also reversible. Further injection of 10 μM Mac1.1, however, induced mass loss with a substantial decrease in Δn_f (Fig. 4B). Dissociation of Mac1.1 resulted in the return of the birefringence Δn_f to a value that was lower than prior to injection. Similar profiles of Δn_f versus m_p to that obtained for 10 μM Mac1.1 were obtained for 20 and 40 μM Mac1.1 binding to DPoPC.

The binding of Mac1.1 to DOPC also resulted in substantial drops in birefringence with increasing mass (Fig. 4C). The Δn_f returned to similar but lower values as Mac1.1 dissociated from DOPC. The disruptive mass loss that was observed on DPoPC at 10 μM Mac1.1 occurred at the higher concentrations of 20 and 40 μM Mac1.1 on DOPC.

Finally, the binding of Mac1.1 to DEPC bilayers (Fig. 4D) induced the largest decrease in birefringence per unit m_p (i.e., the largest drop in birefringence and the lowest amount of peptide bound). The Δn_f values returned to the initial value for the 1.25 and 2.5 μM Mac1.1 dissociation, while the bilayer returned to a less ordered state after the injection of 5–10 μM Mac1.1. Injection of the higher concentrations of 20 and 40 μM Mac1.1 also caused a similar disruptive drop in birefringence as seen for DOPC and DPoPC.

Overall, the extent of birefringence change in each bilayer induced by Mac1.1 binding was proportional to the initial Δn_f values, i.e., the higher the initial Δn_f value of the bilayer, the larger the Δn_f change and, hence, a greater degree of bilayer disorder induced by peptide binding. It is interesting to note, however, that lowest Δn_f value observed was similar for all four bilayers, suggesting that there is a maximum bilayer disorder that can be induced in the immobilized bilayer, irrespective of the initial bilayer thickness and order or the amount of peptide bound.

While each series of birefringence-mass plots in Fig. 4 appears to be a series of reasonably parallel lines, there are two stages at which a discontinuity occurs in the plots which we designate as Stage I, Stage II and Stage III. The concentration at which the transition between each stage was concentration dependent and is listed in Table 2. The transition between Stage I and Stage II was only apparent for DMoPC and DPoPC, occurring at low concentrations of 1.25 μM and 2.5 μM respectively. The transition between Stages II and III was not evident for

Table 2
The structural parameters of supported di-monounsaturated phosphatidylcholine (di-(Cn:1)-PC) bilayer with acyl chain lengths from 14 to 22 carbons at 20 °C.

Lipid bilayer	Stage I → Stage II	Stage II → Stage III
DMoPC	1.25 μM	–
DPoPC	2.5 μM	10 μM
DOPC	–	10–20 μM
DEPC	–	20 μM

DMoPC but occurred at increasing concentrations of 10 μM for DPoPC, 10–20 μM for DOPC and 20 μM for DEPC. These results indicate that there is a significant change in the bilayer order and this change occurs in a co-operative manner at higher concentrations of Mac1.1 with increasing bilayer thickness and order. Thus, a higher concentration of Mac1.1 is required to induce a larger change in bilayer organization with longer acyl chains.

3.4. Effect of Mac1.1 binding on phospholipid dynamics by NMR

The role of the acyl chain length on the membrane activity of the AMP Mac1.1 was further investigated by ^{31}P and ^{1}H solid-state NMR which report on the dynamics of the phospholipid head group and acyl chain, respectively. The intensities of the spinning side bands observed in slow MAS ^{31}P experiments are encoded within the chemical shift anisotropy (CSA) and asymmetry (η) of the phosphorous CSA tensors of the phospholipid head group. The distribution of the CSA and η-values was obtained by using MEMAS, a maximum entropy reconstruction [72]. Mac1.1 did not induce any significant perturbation of the ^{31}P CSA values for DMoPC and DPoPC bilayer membranes. However, there was a small (+ 1.1 ppm) and larger (+ 3.5 ppm) shift towards greater ^{31}P CSA values observed for DOPC and DEPC membranes, respectively. The MEMAS analysis also showed that the CSA values for DMoPC and DEPC were more diverse in the presence of Mac1.1, in particular for DEPC (Fig. 5), indicating the coexistence of different head group conformations or environments. For all systems, the η value was near 0, as expected for such fluid lamellar PC systems undergoing fast re-orientation about the lipid long axis [73], and Mac1.1 did not change this dynamic process.

Table 3
Spin-lattice and spin-spin relaxation times, isotropic chemical shift (***δ***), chemical shift anisotropy and asymmetry (η) derived from ^{31}P NMR experiments[a] of phosphatidylcholine liposomes upon interaction with Mac1.1[b].

	CSA[c] (ppm)	η	***δ***	T_1 (s) ± 0.1 s	T_2 (ms) ± 1.5 ms
DMoPC	29.0	0	− 0.64	1.0	16.1
+ Mac1.1	29.3	0	− 0.72	1.1	13.9
DPoPC	27.9	0	− 0.69	1.1	15.9
+ Mac1.1	27.5	0	− 0.64	1.2	20.1
DOPC	28.4	0	− 0.67	1.1	16.9
+ Mac1.1	29.5	0	− 0.68	1.1	22.3
DEPC	27.5	0	− 0.62	1.1	25.2
+ Mac1.1	31.0	0	− 0.73	1.1	6.5

[a] Spin-lattice (T_1) and spin-spin (T_2) NMR relaxation times and isotropic chemical shift values were obtained at 8 kHz MAS speed. Chemical shift anisotropy (CSA) and asymmetry (η) values were extracted from MEMAS analysis at three spinning speeds (1.6, 1.4 and 0.9 kHz).
[b] All experiments were performed at 25 °C and at a lipid to peptide molar ratio of 25 to 1.
[c] CSA values (i.e., a measure of the largest deviation in chemical shift from the isotropic value) are reported for the highest population obtained by the MEMAS analysis. The full-width powder patter is 1.5 × CSA value.

To further probe the effect of Mac1.1 on the lipid headgroup dynamics, ^{31}P relaxation measurements were performed. The spin-lattice (T_1) relaxation mechanisms are correlated to motions on the nanosecond timescale, typically long axis motion of the phospholipid molecules [72]. As seen in Table 3, all lipid systems showed similar T_1 values, within experimental error, indicating that Mac1.1 has little effect on the long axis rotation of lipids irrespective of the lipid acyl chain length. This further supports the MEMAS results showing no effect on η values. However, the spin-spin (T_2) relaxation measurements, which

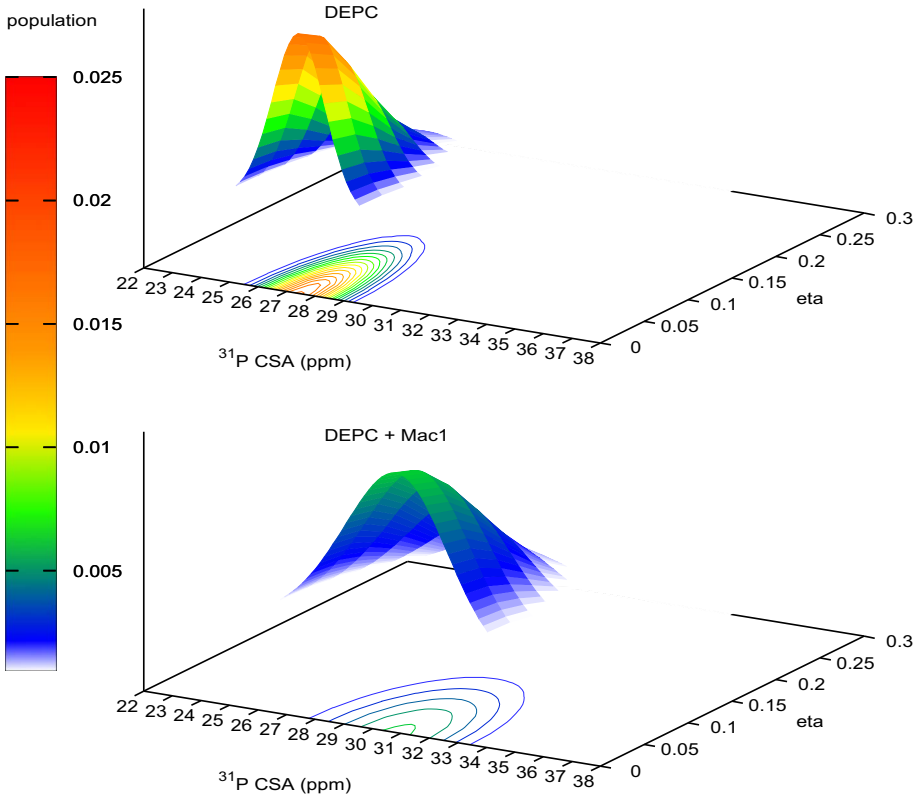

Fig. 5. MEMAS analysis of slow magic angle spinning ^{31}P NMR experiments performed on DEPC multilamellar vesicles (upper panel) and in the presence of Mac1.1 at lipid/peptide molar ratio 25:1 (lower panel). The color code represents the population (total 1.0) for each CSA and η value.

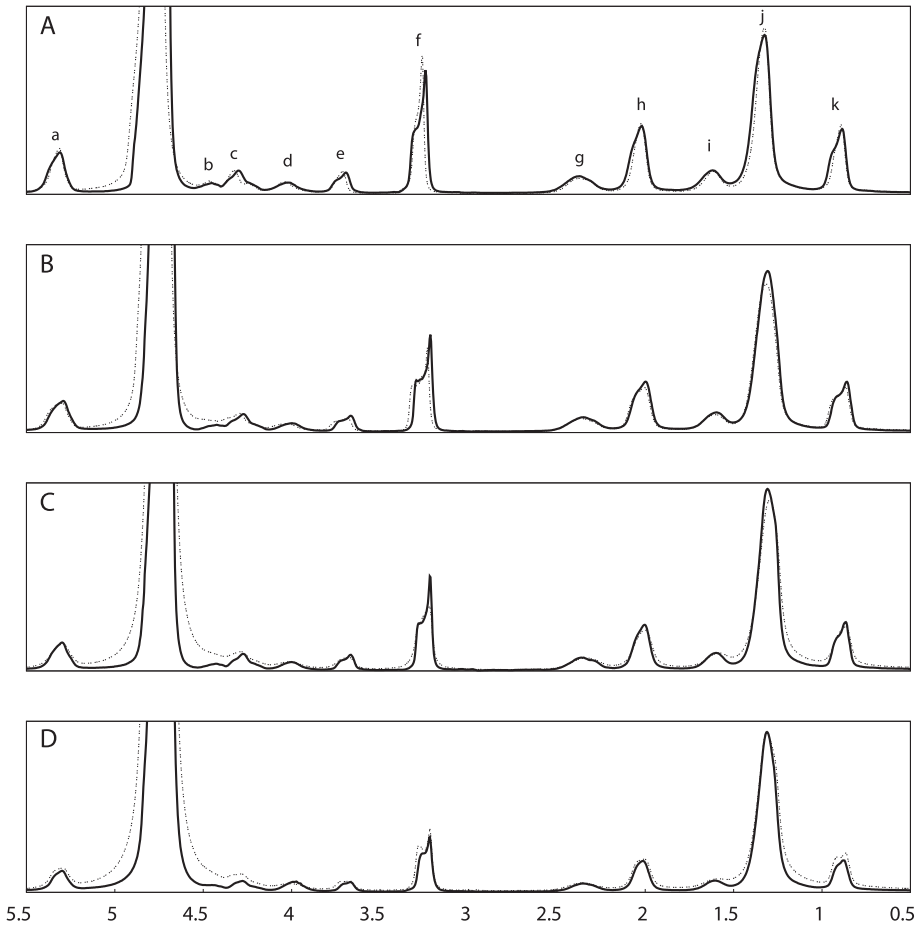

Fig. 6. ^{1}H MAS NMR spectra of: (A) DMoPC, (B) DPoPC, (C) DOPC, and (D) DEPC multilamellar vesicles (—) and in the presence of Mac1.1 at a lipid to peptide molar ratio of 25:1 (———). The assignment of the proton signals are as follow: a) Cg2H and CH═CH, b) Cg1H_2, c) CαH_2, d) Cg3H_2, e) CβH_2, f) N$(CH_3)_3$, g) C2H_2, h) $\underline{CH_2}CH{=}CH\underline{CH_2}$, i) C3$H_2$, j) $(CH_2)_n$, k) CH_3 [ref]. The peak around 4.7 ppm is from the water signal.

are correlated to millisecond timescale motions such as membrane wobbling [72], exhibited different modulation depending on the lipid acyl chain length. While the T_2 value obtained for the short chain DMoPC decreased slightly in the presence of Mac1.1, peptide binding induced larger increases in T_2 values for the longer chain DPoPC and DOPC bilayers. In contrast, Mac1.1 binding significantly decreased T_2 values for DEPC (~70%), which suggests greater disordering for the longest lipid, with an increase in low frequency motion and correlates with the increased disorder induced by Mac1.1 binding observed by DPI and may reflect greater peptide binding/incorporation with the longer PC.

Magic angle spinning ^{1}H NMR experiments were performed to localize the perturbation induced by Mac1.1 along the lipid structure (Fig. 6). For DMoPC, the headgroup ^{1}H signals were perturbed by the presence of Mac1.1, with a slight upfield shift (Fig. 6A, c, e–f) and a slight decrease in the overall signal linewidths. The peptide induced similar but smaller effects on the ^{1}H signals of DPoPC, although the acyl chain signals were not sharpened. For DOPC and DEPC, the only observed effect of the peptide was to slightly broaden the ^{1}H linewidths, especially for the acyl chain ^{1}H signals (Fig. 6C & D, i–k) and which may be due to the decrease in T_2 as reported by ^{31}P NMR. However, it is difficult to resolve small chemical shift changes in phospholipids by ^{1}H solid-state NMR [74] and peptides rarely produce dramatic changes unless there is a phase change. Nevertheless, the change in linewidth indicated an effect on the acyl chains which suggests that the AMP is inserted into the bilayer and that differences in the hydrophobic core results in differences in linewidth perturbation.

Overall, the NMR results suggest that Mac1.1 has a different interaction depending on the hydrophobic thickness of the lipid membrane. The greatest mismatch would appear to be for DEPC lipids, based on the changes in ^{31}P NMR data. Furthermore, there were no indications of non-bilayer structures caused by the peptide insertion into fluid lipid bilayers, regardless of the acyl chain length for monounsaturated PC.

4. Discussion

Bacterial membranes have been recognized as the main targets for the bactericidal activity of most AMPs and the majority of studies on their interaction with membranes have focused mainly on the structural and topological changes of the peptides and perturbation of membrane integrity. While there are several peptide structural properties that contribute to the overall selectivity and destabilization of membranes, more focus on the specific structural features of the bilayer that control AMP action, particularly in terms of chemical composition and physical organization, is needed. Indeed, the evolution of bacterial resistance against host AMPs has been linked to changes in the lipid composition and modification and changes in membrane fluidity [17,75,76]. In order to delineate the mechanisms of AMP action and resistance, it is important to quantitatively characterize the dynamic changes in membrane structure in response to AMPs.

In this study, planar solid-supported unilamellar bilayer systems of four di-monounsaturated phosphatidylcholines with acyl chain lengths between 14 and 22 carbons, were characterised by DPI to explore the effect of a range of structural parameters, including thickness, mass, surface area per lipid and order, on the binding of the AMP Mac1.1. The thickness values for these lipid bilayers (Table 1) increased with increasing acyl chain length and correlate well with the thickness values obtained by X-ray and neutron scattering [63,64,68]. Earlier studies have also shown that PC bilayer thickness increased linearly with saturated acyl chain length between 12 and 18 carbons [67,68] and for monounsaturated acyl chains from 18 to 24 carbons [70]. In this study, the DPI results showed that the bilayer thickness for each

monounsaturated acyl chain from 14 to 22 carbons corresponded to 1.9 Å per CH_2 group, which also correlates well with the value reported for a series of bilayer thickness values collected from scattering data [67,68]. The unsaturated acyl chains also exerted a significant effect on thickness and packing order. By comparison with previous studies with different degrees of unsaturation, the bilayer thickness and order in this present study was significantly reduced relative to fully saturated DMPC [52,62] and the mono-unsaturated POPC [77,78]. In addition, the thickness and birefringence values for DMoPC and DPoPC in this study were also much less than those obtained for the fully saturated DMPC and the mono-unsaturated POPC (with the same acyl chain length in both gel and fluid phase), respectively [40,52].

The effect of acyl chain length and unsaturation on the binding behavior of Mac1.1 was then assessed with neutral PC SLBs. In particular, we sought to investigate the influence of membrane order on the binding behavior of Mac1.1. While alterations in lipid organization may cause changes in the ability of AMPs to insert into the membrane, at present, there is no clear understanding of the mechanism of how changes in acyl chain length and saturation affect the membrane structural properties and reduce susceptibility of bacteria to AMPs.

Overall, the results suggest that Mac1.1 bound to each lipid bilayer in a surface orientation, but there were differences in the response of the bilayer to the levels of bound peptide. The overall binding process can be examined in terms of: 1) the amount of Mac1.1 bound to each lipid bilayer, and 2) the corresponding changes in bilayer packing during this interaction. The results indicated that there was a significant difference between the maximum amount of Mac1.1 that bound to each bilayer and the amount of peptide needed to disturb the bilayer. Firstly, as summarized in Fig. 7, there was a biphasic dependency between the amount of bound Mac1.1 and bilayer thickness, with a discontinuity in the dependency from C14 to C16 and from C16 to C22. Thus, at lower peptide concentrations (between 1.25 and 10 μM Mac1.1), there was an increase in bound peptide from C14 to C16, while at the higher concentrations of 20 and 40 μM Mac1.1, the amount of peptide bound decreased with increasing chain length from C14 to C16 (Fig. 7). In comparison, there was a decrease in the amount of bound Mac1.1 from C16 to C22 at all peptide concentrations. These results suggest that there is a threshold bilayer ordering and thickness above which no further peptide binds. The results suggest that the thinner bilayer may be able to adsorb more peptide before the bilayer packing/order is compromised. In addition, the smaller area per lipid may allow more peptide to be adsorbed.

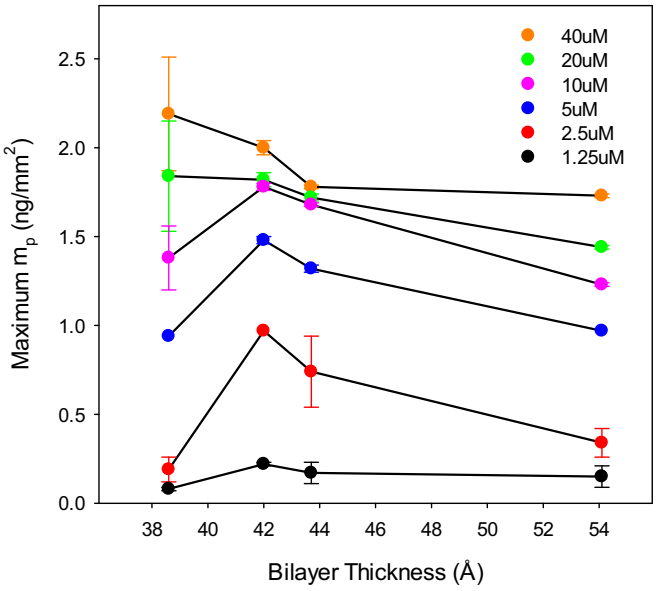

Fig. 7. The dependence of maximum bilayer-bound Mac1.1 mass on the bilayer thickness of di-monounsaturated PC bilayers at peptide concentrations ranging from 1.25 to 40 μM.

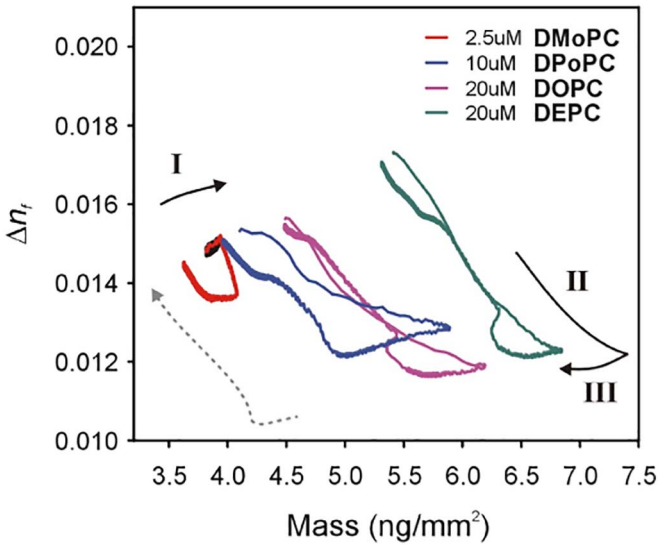

Fig. 8. Schematic of discrete stages (I, II and III) of changes in PC bilayer packing order upon Mac1.1 binding.

In terms of the changes in bilayer ordering, the mass-birefringence plots in Fig. 4 revealed the existence of three stages in membrane disordering upon Mac1.1 binding, the features of which are summarized in Fig. 8. The early stage transition (Stage I → Stage II) was only evident with the shorter chain bilayers while the later stage transition (Stage II → Stage III) occurred with the three thicker bilayers but at increasingly higher peptide loadings. In terms of the bilayer properties, the thickness and order of each of the four bilayers in this study increased linearly with increasing acyl chain length (Fig. 1), while the results of the ^{31}P and ^{1}H NMR experiments indicated that Mac1.1 binds to the surface or interface of each of the four bilayers. These results are consistent with our previous NMR study which indicated that Mac1.1 also bound to the surface of the DMPC bilayer in both the gel and fluid state [40]. In addition, the T_1 and T_2 data suggests that the acyl chains also undergo increased perturbation upon Mac1.1 binding which may correspond to the transitions observed in the birefringence-mass plots (Fig. 4). Overall therefore, the results suggest that the first transition between Stage I and Stage II may relate to the initial binding of Mac1.1 and followed by Stage II which may correspond to reversible bending motion of the lipid acyl chains to accommodate Mac1.1 at the interfacial region. Finally, Stage III may correspond to a lateral expansion at high peptide loadings as Mac1.1 starts to insert into the bilayer and which we have previously observed for other membrane-active peptides [47,78].

We have also previously shown that the fully saturated DMPC is more susceptible in the gel state to destabilization by Mac1.1, and this disruption was partially reversible as evidenced by isotropic ^{31}P and ^{2}H NMR signals and decrease in birefringence [40]. Ramamoorthy and coworkers showed hexagonal phase formation by ^{31}P NMR at high concentrations of AMPs, MSI-78 [79] and LL-37 [80] (but this was in DOPE rather than a PC lipid). They later showed a detergent-like mechanism for MSI in large unilamellar vesicles (Lee et al. 2015, Biochemistry).

By comparison, the changes in mass and birefringence for Mac1.1 binding to the four di-unsaturated phospholipids used in this study revealed multiple states of bilayer order, with Stage II almost fully reversible. Moreover, the more fluid chains of these lipids inhibited the formation of an isotropic lipid phase in the presence of Mac1.1 as reported by the ^{31}P NMR data. Furthermore, ^{31}P NMR data showed a significant change in the head group dynamics of DEPC in the presence Mac1.1 compared to the thinner membranes while the head group dynamics in DMoPC and DPoPC were not as affected but the acyl chains experienced greater dynamics (sharper ^{1}H signals), supporting a

slightly deeper location of Mac1.1 in thinner membranes.

Oligomer formation has also been proposed to impact on the lytic activity of Mac1.1 and may be influenced by the thickness of the PC bilayer, whereby small oligomers may tilt in thinner membranes while larger Mac1.1 oligomers may form in thicker membranes [45]. This correlates with the increased perturbation seen in the thicker bilayer and may occur to some extent at higher peptide concentrations. In addition, while the concept of hydrophobic mismatch has been used to describe peptide orientation of transmembrane peptides, the multiple bilayer states evident in the current study suggest that hydrophobic matching is a dynamic process involving on-going changes in peptide topological states and/or adaptions of the lipid packing order. The helical structure of Mac1.1 has been shown to vary between ~60–75% with fully saturated lipids of different thickness [44] while addition of cholesterol inhibited Mac1.1 binding, leaving the peptide mostly unstructured and preventing significant dye release from vesicles [44]. As cholesterol increases the order of fluid bilayers, this further illustrates how fluidity combined with changes in the membrane thickness modulates AMP activity. Moreover, a recent study has demonstrated that the membrane thickness determines the location of cholesterol in model membranes, further illustrating the role of bilayer thickness in modulating the organization of membrane components [81]. In addition, the bound topological state of PGLa and other transmembrane peptides has been reported whereby the peptides were mainly oriented parallel to the thicker membrane surface but tilted in thinner membranes [46].

Taken together, our current results indicate that the thicker and more ordered the bilayer, the higher the amount of peptide required to disrupt (or insert into) the bilayer. In addition, the more flexible di-unsaturated lipids exhibit a greater capacity to remodel in terms of bending and/or expansion in response to AMP binding.

5. Conclusion

Since bacteria can modulate the degree of unsaturation during their growth phase or upon external stimuli [18,22], changes in membrane lipids may lead to AMP resistance. A benefit of AMPs, however, is that they do not readily target cholesterol-rich eukaryotic cell membranes over bacterial membranes. Hydrophobic mismatch and lipid order affect the topological states, mass threshold for membrane destabilization, helical content and/or oligomerization of AMPs, which strongly govern the mechanism of action of Mac1.1. In this study, we have characterised the capacity of the bilayer to adapt and respond to Mac1.1 binding and the thinner membranes are less able to adapt/adjust than the thicker membranes to peptide binding. While the composition of bacterial membranes is more complex than the model systems used here, given that neutralization of bilayer surface charge is a mechanism used to make membranes resistant to AMPs, the present study indicates that changes in the acyl chain compositions of bacterial membrane lipids can also underpin resistance mechanisms to AMPs.

Transparency document

The Transparency document associated with this article can be found, in online version.

Acknowledgements

The authors gratefully acknowledge the support of the Australian Research Council Discovery Grant DP110101866 and the National Health and Medical Research Council Project Grant ID#1044327.

References

[1] R. Laxminarayan, A. Duse, C. Wattal, A.K. Zaidi, H.F. Wertheim, N. Sumpradit, E. Vlieghe, G.L. Hara, I.M. Gould, H. Goossens, C. Greko, A.D. So, M. Bigdeli, G. Tomson, W. Woodhouse, E. Ombaka, A.Q. Peralta, F.N. Qamar, F. Mir, S. Kariuki, Z.A. Bhutta, A. Coates, R. Bergstrom, G.D. Wright, E.D. Brown, O. Cars, Antibiotic resistance-the need for global solutions, Lancet Infect. Dis. 13 (2013) 1057–1098.
[2] A.H. Holmes, L.S. Moore, A. Sundsfjord, M. Steinbakk, S. Regmi, A. Karkey, P.J. Guerin, L.J. Piddock, Understanding the mechanisms and drivers of antimicrobial resistance, Lancet 387 (2016) 176–187.
[3] Tackling Drug-Resistant Infections Globally, Final report and recommendations, review on antimicrobial resistance, https://amr-review.org, (2016).
[4] D. Campoccia, L. Montanaro, C.R. Arciola, A review of the biomaterials technologies for infection-resistant surfaces, Biomaterials 34 (2013) 8533–8554.
[5] M.J. Hajipour, K.M. Fromm, A.A. Ashkarran, D. Jimenez de Aberasturi, I.R. de Larramendi, T. Rojo, V. Serpooshan, W.J. Parak, M. Mahmoudi, Antibacterial properties of nanoparticles, Trends Biotechnol. 30 (2012) 499–511.
[6] N. Beyth, Y. Houri-Haddad, A. Domb, W. Khan, R. Hazan, Alternative antimicrobial approach: nano-antimicrobial materials, Evid. Based Complement. Alternat. Med. 2015 (2015) 246012.
[7] P. Dutta, S. Das, Mammalian antimicrobial peptides: promising therapeutic targets against infection and chronic inflammation, Curr. Top. Med. Chem. 16 (2016) 99–129.
[8] C.D. Fjell, J.A. Hiss, R.E. Hancock, G. Schneider, Designing antimicrobial peptides: form follows function, Nat. Rev. Drug Discov. 11 (2011) 37–51.
[9] S. Ruer, N. Pinotsis, D. Steadman, G. Waksman, H. Remaut, Virulence-targeted antibacterials: concept, promise, and susceptibility to resistance mechanisms, Chem. Biol. Drug Des. 86 (2015) 379–399.
[10] D. Maura, A.E. Ballok, L.G. Rahme, Considerations and caveats in anti-virulence drug development, Curr. Opin. Microbiol. 33 (2016) 41–46.
[11] A.C. Rios, C.G. Moutinho, F.C. Pinto, F.S. Del Fiol, A. Jozala, M.V. Chaud, M.M. Vila, J.A. Teixeira, V.M. Balcao, Alternatives to overcoming bacterial resistances: state-of-the-art, Microbiol. Res. 191 (2016) 51–80.
[12] L. Czaplewski, R. Bax, M. Clokie, M. Dawson, H. Fairhead, V.A. Fischetti, S. Foster, B.F. Gilmore, R.E. Hancock, D. Harper, I.R. Henderson, K. Hilpert, B.V. Jones, A. Kadioglu, D. Knowles, S. Olafsdottir, D. Payne, S. Projan, S. Shaunak, J. Silverman, C.M. Thomas, T.J. Trust, P. Warn, J.H. Rex, Alternatives to antibiotics-a pipeline portfolio review, Lancet Infect. Dis. 16 (2016) 239–251.
[13] C. Bebbington, G. Yarranton, Antibodies for the treatment of bacterial infections: current experience and future prospects, Curr. Opin. Biotechnol. 19 (2008) 613–619.
[14] R. Dagan, K.P. Klugman, Impact of conjugate pneumococcal vaccines on antibiotic resistance, Lancet Infect. Dis. 8 (2008) 785–795.
[15] Y. Shai, Mode of action of membrane active antimicrobial peptides, Biopolymers 66 (2002) 236–248.
[16] M.A. Sani, F. Separovic, How membrane-active peptides get into lipid membranes, Acc. Chem. Res. 49 (2016) 1130–1138.
[17] S. Omardien, S. Brul, S.A. Zaat, Antimicrobial activity of cationic antimicrobial peptides against gram-positives: current progress made in understanding the mode of action and the response of bacteria, Front. Cell Dev. Biol. 4 (2016) 111.
[18] S. Maria-Neto, K.C. de Almeida, M.L. Macedo, O.L. Franco, Understanding bacterial resistance to antimicrobial peptides: from the surface to deep inside, Biochim. Biophys. Acta 1848 (2015) 3078–3088.
[19] R. Nuri, T. Shprung, Y. Shai, Defensive remodeling: how bacterial surface properties and biofilm formation promote resistance to antimicrobial peptides, Biochim. Biophys. Acta 1848 (2015) 3089–3100.
[20] D.I. Andersson, D. Hughes, J.Z. Kubicek-Sutherland, Mechanisms and consequences of bacterial resistance to antimicrobial peptides, Drug Resist. Updat. 26 (2016) 43–57.
[21] A.S. Bayer, T. Schneider, H.G. Sahl, Mechanisms of daptomycin resistance in *Staphylococcus aureus*: role of the cell membrane and cell wall, Ann. N. Y. Acad. Sci. 1277 (2013) 139–158.
[22] R. Kumariya, S.K. Sood, Y.S. Rajput, N. Saini, A.K. Garsa, Increased membrane surface positive charge and altered membrane fluidity leads to cationic antimicrobial peptide resistance in *Enterococcus faecalis*, Biochim. Biophys. Acta 1848 (2015) 1367–1375.
[23] A. Peschel, H.G. Sahl, The co-evolution of host cationic antimicrobial peptides and microbial resistance, Nat. Rev. Microbiol. 4 (2006) 529–536.
[24] A.S. Bayer, R. Prasad, J. Chandra, A. Koul, M. Smriti, A. Varma, R.A. Skurray, N. Firth, M.H. Brown, S.P. Koo, M.R. Yeaman, In vitro resistance of *Staphylococcus aureus* to thrombin-induced platelet microbicidal protein is associated with alterations in cytoplasmic membrane fluidity, Infect. Immun. 68 (2000) 3548–3553.
[25] P. Lather, A.K. Mohanty, P. Jha, A.K. Garsa, S.K. Sood, Changes associated with cell membrane composition of *Staphylococcus aureus* on acquisition of resistance against class IIa bacteriocin and its in vitro substantiation, Eur. Food Res. Technol. 240 (2015) 101–107.
[26] N.N. Mishra, A.S. Bayer, T.T. Tran, Y. Shamoo, E. Mileykovskaya, W. Dowhan, Z. Guan, C.A. Arias, Daptomycin resistance in enterococci is associated with distinct alterations of cell membrane phospholipid content, PLoS One 7 (2012) e43958.
[27] T. Rozek, R.J. Waugh, S.T. Steinborner, J.H. Bowie, M.J. Tyler, J.C. Wallace, The maculatin peptides from the skin glands of the tree frog *Litoria genimaculata*: a comparison of the structures and antibacterial activities of maculatin 1.1 and caerin 1.1, J. Pept. Sci. 4 (1998) 111–115.
[28] M.A. Apponyi, T.L. Pukala, C.S. Brinkworth, V.M. Maselli, J.H. Bowie, M.J. Tyler, G.W. Booker, J.C. Wallace, J.A. Carver, F. Separovic, J. Doyle, L.E. Llewellyn, Host-defence peptides of Australian anurans: structure, mechanism of action and evolutionary significance, Peptides 25 (2004) 1035–1054.
[29] M.P. Boland, F. Separovic, Membrane interactions of antimicrobial peptides from Australian tree frogs, Biochim. Biophys. Acta 1758 (2006) 1178–1183.
[30] B.C. Chia, J.A. Carver, T.D. Mulhern, J.H. Bowie, Maculatin 1.1, an anti-microbial peptide from the Australian tree frog, *Litoria genimaculata* solution structure and

biological activity, Eur. J. Biochem. 267 (2000) 1894–1908.
[31] D.I. Fernandez, J.D. Gehman, F. Separovic, Membrane interactions of antimicrobial peptides from Australian frogs, Biochim. Biophys. Acta 1788 (2009) 1630–1638.
[32] T. Niidome, K. Kobayashi, H. Arakawa, T. Hatakeyama, H. Aoyagi, Structure-activity relationship of an antibacterial peptide, maculatin 1.1, from the skin glands of the tree frog, *Litoria genimaculata*, J. Pept. Sci. 10 (2004) 414–422.
[33] C.S. Brinkworth, J.H. Bowie, Negative ion electrospray mass spectra of the maculatin peptides from the tree frogs *Litoria genimaculata* and *Litoria eucnemis*, Rapid Commun. Mass Spectrom. 17 (2003) 2215–2225.
[34] S.E. VanCompernolle, R.J. Taylor, K. Oswald-Richter, J. Jiang, B.E. Youree, J.H. Bowie, M.J. Tyler, J.M. Conlon, D. Wade, C. Aiken, T.S. Dermody, V.N. KewalRamani, L.A. Rollins-Smith, D. Unutmaz, Antimicrobial peptides from amphibian skin potently inhibit human immunodeficiency virus infection and transfer of virus from dendritic cells to T cells, J. Virol. 79 (2005) 11598–11606.
[35] G.W. Seto, S. Marwaha, D.M. Kobewka, R.N. Lewis, F. Separovic, R.N. McElhaney, Interactions of the Australian tree frog antimicrobial peptides aurein 1.2, citropin 1.1 and maculatin 1.1 with lipid model membranes: differential scanning calorimetric and Fourier transform infrared spectroscopic studies, Biochim. Biophys. Acta 1768 (2007) 2787–2800.
[36] C.S. Chia, J. Torres, M.A. Cooper, I.T. Arkin, J.H. Bowie, The orientation of the antibiotic peptide maculatin 1.1 in DMPG and DMPC lipid bilayers. Support for a pore-forming mechanism, FEBS Lett. 512 (2002) 47–51.
[37] K. Hall, H. Mozsolits, M.-I. Aguilar, Surface plasmon resonance analysis of antimicrobial peptide-membrane interactions: affinity & mechanism of action, Lett. Pept. Sci. 10 (2003) 475–485.
[38] E.E. Ambroggio, F. Separovic, J. Bowie, G.D. Fidelio, Surface behaviour and peptide-lipid interactions of the antibiotic peptides, maculatin and citropin, Biochim. Biophys. Acta 1664 (2004) 31–37.
[39] D.I. Fernandez, A.P. Le Brun, T.H. Lee, P. Bansal, M.I. Aguilar, M. James, F. Separovic, Structural effects of the antimicrobial peptide maculatin 1.1 on supported lipid bilayers, Eur. Biophys. J. 42 (2013) 47–59.
[40] D.I. Fernandez, T.H. Lee, M.A. Sani, M.I. Aguilar, F. Separovic, Proline facilitates membrane insertion of the antimicrobial peptide maculatin 1.1 via surface indentation and subsequent lipid disordering, Biophys. J. 104 (2013) 1495–1507.
[41] T.H. Lee, C. Heng, F. Separovic, M.I. Aguilar, Comparison of reversible membrane destabilisation induced by antimicrobial peptides derived from Australian frogs, Biochim. Biophys. Acta 1838 (2014) 2205–2215.
[42] M.A. Sani, E. Gagne, J.D. Gehman, T.C. Whitwell, F. Separovic, Dye-release assay for investigation of antimicrobial peptide activity in a competitive lipid environment, Eur. Biophys. J. 43 (2014) 445–450.
[43] D.I. Fernandez, M.-A. Sani, F. Separovic, Interactions of the antimicrobial peptide maculatin 1.1 and analogues with phospholipid bilayers, Aust. J. Chem. 64 (2011) 798–805.
[44] M.A. Sani, T.C. Whitwell, F. Separovic, Lipid composition regulates the conformation and insertion of the antimicrobial peptide maculatin 1.1, Biochim. Biophys. Acta 1818 (2012) 205–211.
[45] Y. Wang, C.H. Chen, D. Hu, M.B. Ulmschneider, J.P. Ulmschneider, Spontaneous formation of structurally diverse membrane channel architectures from a single antimicrobial peptide, Nat. Commun. 7 (2016) 13535.
[46] E.S. Salnikov, B. Bechinger, Lipid-controlled peptide topology and interactions in bilayers: structural insights into the synergistic enhancement of the antimicrobial activities of PGLa and magainin 2, Biophys. J. 100 (2011) 1473–1480.
[47] D.J. Hirst, T.H. Lee, M.J. Swann, S. Unabia, Y. Park, K.S. Hahm, M.I. Aguilar, Effect of acyl chain structure and bilayer phase state on binding and penetration of a supported lipid bilayer by HPA3, Eur. Biophys. J. 40 (2011) 503–514.
[48] T.H. Lee, K.N. Hall, M.I. Aguilar, Antimicrobial peptide structure and mechanism of action: a focus on the role of membrane structure, Curr. Top. Med. Chem. 16 (2016) 25–39.
[49] J. Escorihuela, M.A. Gonzalez-Martinez, J.L. Lopez-Paz, R. Puchades, A. Maquieira, D. Gimenez-Romero, Dual-polarization interferometry: a novel technique to light up the nanomolecular world, Chem. Rev. 115 (2015) 265–294.
[50] K. Hall, T.H. Lee, A.I. Mechler, M.J. Swann, M.I. Aguilar, Real-time measurement of membrane conformational states induced by antimicrobial peptides: balance between recovery and lysis, Sci Rep 4 (2014) 5479.
[51] T.H. Lee, K.N. Hall, M.J. Swann, J.F. Popplewell, S. Unabia, Y. Park, K.S. Hahm, M.I. Aguilar, The membrane insertion of helical antimicrobial peptides from the N-terminus of helicobacter pylori ribosomal protein L1, Biochim. Biophys. Acta 1798 (2010) 544–557.
[52] T.H. Lee, C. Heng, M.J. Swann, J.D. Gehman, F. Separovic, M.I. Aguilar, Real-time quantitative analysis of lipid disordering by aurein 1.2 during membrane adsorption, destabilisation and lysis, Biochim. Biophys. Acta 1798 (2010) 1977–1986.
[53] G.H. Cross, A.A. Reeves, S. Brand, J.F. Popplewell, L.L. Peel, M.J. Swann, N.J. Freeman, A new quantitative optical biosensor for protein characterisation, Biosens. Bioelectron. 19 (2003) 383–390.
[54] M.J. Swann, L.L. Peel, S. Carrington, N.J. Freeman, Dual-polarization interferometry: an analytical technique to measure changes in protein structure in real time, to determine the stoichiometry of binding events, and to differentiate between specific and nonspecific interactions, Anal. Biochem. 329 (2004) 190–198.
[55] R. Horvath, J.J. Ramsden, Quasi-isotropic analysis of anisotropic thin films on optical waveguides, Langmuir 23 (2007) 9330–9334.
[56] J.J. Ramsden, Molecular orientation in lipid bilayers, Philos. Mag. B 79 (1999) 381–386.
[57] N. Sinha, C.V. Grant, C.H. Wu, A.A. De Angelis, S.C. Howell, S.J. Opella, SPINAL modulated decoupling in high field double- and triple-resonance solid-state NMR experiments on stationary samples, J. Magn. Reson. 177 (2005) 197–202.
[58] G. Bodenhausen, R. Freeman, D.L. Turner, Suppression of artifacts in two-dimensional J spectroscopy, J. Magn. Reson. 27 (1977) 511–514.
[59] E.L. Hahn, D.E. Maxwell, Spin Echo measurements of nuclear spin coupling in molecules, Phys. Rev. 88 (1952) 1070–1084.
[60] M.A. Sani, F. Separovic, J.D. Gehman, Disentanglement of heterogeneous dynamics in mixed lipid systems, Biophys. J. 100 (2011) L40–42.
[61] M. Bak, J.T. Rasmussen, N.C. Nielsen, SIMPSON: a general simulation program for solid-state NMR spectroscopy, J. Magn. Reson. 147 (2000) 296–330.
[62] A. Mashaghi, M. Swann, J. Popplewell, M. Textor, E. Reimhult, Optical anisotropy of supported lipid structures probed by waveguide spectroscopy and its application to study of supported lipid bilayer formation kinetics, Anal. Chem. 80 (2008) 3666–3676.
[63] N. Kucerka, J. Gallova, D. Uhrikova, P. Balgavy, M. Bulacu, S.J. Marrink, J. Katsaras, Areas of monounsaturated diacylphosphatidylcholines, Biophys. J. 97 (2009) 1926–1932.
[64] N. Kucerka, S. Tristram-Nagle, J.F. Nagle, Structure of fully hydrated fluid phase lipid bilayers with monounsaturated chains, J. Membr. Biol. 208 (2005) 193–202.
[65] N. Kucerka, J.F. Nagle, J.N. Sachs, S.E. Feller, J. Pencer, A. Jackson, J. Katsaras, Lipid bilayer structure determined by the simultaneous analysis of neutron and X-ray scattering data, Biophys. J. 95 (2008) 2356–2367.
[66] J. Gallova, D. Uhrikova, N. Kucerka, J. Teixeira, P. Balgavy, Hydrophobic thickness, lipid surface area and polar region hydration in monounsaturated diacylphosphatidylcholine bilayers: SANS study of effects of cholesterol and beta-sitosterol in unilamellar vesicles, Biochim. Biophys. Acta 1778 (2008) 2627–2632.
[67] B.A. Cornell, F. Separovic, Membrane thickness and acyl chain length, Biochim. Biophys. Acta 733 (1983) 189–193.
[68] N. Kucerka, F.A. Heberle, J. Pan, J. Katsaras, Structural significance of lipid diversity as studied by small angle neutron and X-ray scattering, Membranes (Basel, Switz.) 5 (2015) 454–472.
[69] F. Dumas, M.C. Lebrun, J.F. Tocanne, Is the protein/lipid hydrophobic matching principle relevant to membrane organization and functions? FEBS Lett. 458 (1999) 271–277.
[70] B.A. Lewis, D.M. Engelman, Lipid bilayer thickness varies linearly with acyl chain length in fluid phosphatidylcholine vesicles, J. Mol. Biol. 166 (1983) 211–217.
[71] T.H. Lee, D.J. Hirst, M.I. Aguilar, New insights into the molecular mechanisms of biomembrane structural changes and interactions by optical biosensor technology, Biochim. Biophys. Acta 1848 (2015) 1868–1885.
[72] M.A. Sani, F. Separovic, Progression of NMR studies of membrane-active peptides from lipid bilayers to live cells, J. Magn. Reson. 253 (2015) 138–142.
[73] D.K. Weber, M.A. Sani, M.T. Downton, F. Separovic, F.R. Keene, J.G. Collins, Membrane insertion of a dinuclear polypyridylruthenium(II) complex revealed by solid-state NMR and molecular dynamics simulation: implications for selective antibacterial activity, J. Am. Chem. Soc. 138 (2016) 15267–15277.
[74] A. Ramamoorthy, J. Xu, 2D 1H/1H RFDR and NOESY NMR experiments on a membrane-bound antimicrobial peptide under magic angle spinning, J. Phys. Chem. B 117 (2013) 6693–6700.
[75] N.N. Mishra, A.S. Bayer, Correlation of cell membrane lipid profiles with daptomycin resistance in methicillin-resistant *Staphylococcus aureus*, Antimicrob. Agents Chemother. 57 (2013) 1082–1085.
[76] H.-G. Sahl, Y. Shai, Bacterial resistance to antimicrobial peptides, Biochim. Biophys. Acta Biomembr. 1848 (2015) 3019–3020.
[77] D.J. Hirst, T.H. Lee, K. Kulkarni, J.A. Wilce, M.I. Aguilar, The impact of cell-penetrating peptides on membrane bilayer structure during binding and insertion, Biochim. Biophys. Acta 1858 (2016) 1841–1849.
[78] D.J. Hirst, T.H. Lee, M.J. Swann, M.I. Aguilar, Combined mass and structural kinetic analysis of multistate antimicrobial peptide-membrane interactions, Anal. Chem. 85 (2013) 9296–9304.
[79] K.J. Hallock, D.K. Lee, A. Ramamoorthy, MSI-78, an analogue of the magainin antimicrobial peptides, disrupts lipid bilayer structure via positive curvature strain, Biophys. J. 84 (2003) 3052–3060.
[80] K.A. Henzler Wildman, D.K. Lee, A. Ramamoorthy, Mechanism of lipid bilayer disruption by the human antimicrobial peptide, LL-37, Biochemistry 42 (2003) 6545–6558.
[81] D. Marquardt, F.A. Heberle, D.V. Greathouse, R.E. Koeppe, R.F. Standaert, B.J. Van Oosten, T.A. Harroun, J.J. Kinnun, J.A. Williams, S.R. Wassall, J. Katsaras, Lipid bilayer thickness determines cholesterol's location in model membranes, Soft Matter 12 (2016) 9417–9428.